

Microwave-assisted synthesis, spectral characterization and DFT studies of Zn(II) complexes based on *N*-acylhydrazone ligands: stability and antioxidant activity

Daniela C. Santos^{1,2}, Ruan R. Henriques², Marcos A. A. Lopes Jr.^{1,3}, Paulo J. S. Maia^{1,4}, Andreza M. B. da Silva⁴, Diego F. S. Paschoal¹ and Andréa L. F. de Souza^{1,3,*}

¹ Universidade Federal do Rio de Janeiro, Campus Macaé Professor Aloísio Teixeira, CEP 27930-560, Macaé – RJ – Brazil

² Universidade Federal do Rio de Janeiro, Instituto de Macromoléculas, Cidade Universitária, CEP 21941-598, Rio de Janeiro – RJ – Brazil

³ Universidade Federal do Rio de Janeiro, Instituto de Química, Cidade Universitária, CEP 21941-909, Rio de Janeiro – RJ – Brazil

⁴ Universidade Federal do Amazonas, Programa de Pós-Graduação em Ciência e Tecnologia para Recursos Amazônicos (PPGCTRA), CEP 69103-128, Itacoatiara – AM – Brazil

Abstract: This article reports the synthesis of seven Zn(II) complexes containing *N*-acylhydrazone ligands (**L1** to **L7**) and the assessment of their antioxidant. Microwave assisted-synthesis of ligands with ZnCl₂ in MeOH yielded tetrahedral Zn(II) complexes with a 1:2 metal: ligand ratio, characterized by HRMS, FTIR, and UV-Vis spectroscopy, thermal and electrochemical analyses, and DFT calculations. The (**L3**)₂Zn complex exhibited the lowest thermal stability, and (**L6**)₂Zn and (**L7**)₂Zn were the most stable. XRD powder showed that all complexes have good crystallinity with crystalline dimensions ranging from 32 to 86 nm. Cyclic voltammetry of Zn(II) complexes indicated a reversible redox process for (**L4**)₂Zn and an irreversible process for the remaining six complexes: (**L1**)₂Zn to (**L3**)₂Zn and (**L5**)₂Zn to (**L7**)₂Zn. Antioxidant activity of ligands and complexes was assessed by the DPPH method; the **L7** ligand and corresponding (**L7**)₂Zn complex exhibited good activity, IC₅₀ = 65.30 μmol.l⁻¹ and 78.70 μmol.l⁻¹, respectively, when compared with standard ascorbic acid.

Keywords: Zinc; *N*-acylhydrazone; isoniazid; microwave; antioxidant.

1. Introduction

Hydrazones and *N*-acylhydrazones have a -C=N-NH- structure and are generally derived from a condensation reaction between hydrazines and aldehydes (or ketones) and the latter from hydrazides.. Due to their physicochemical properties, *N*-acylhydrazones have drawn much scientific and societal interest for various industrial, biological, pharmacological, therapeutic, and technological applications¹.

Hydrazones and *N*-acylhydrazones have desirable properties, such as flexibility and versatility, rendered by their carbonyl group. Due to these characteristics, these substances have been employed to detect metal ions and used as chelating agents to produce different stable complexes with transition metals². In addition, the non-oxygen binding pairs of electrons of the carbonyl group present in *N*-acylhydrazones constitute good active sites, given that polydentate

chelators increase the stability of the complex formed³⁻⁶.

The chromophore azomethine is responsible for forming these active sites in *N*-acylhydrazones, allowing a variety of coordination and geometries while maintaining high stability. In addition, interconnected nitrogen promotes coordination with the neutral and deprotonated forms, increasing the possibility of complex formation⁷⁻¹².

Zinc is an element of the fifth period of the periodic table whose *d* orbital is filled, i.e., a *d*¹⁰ metal. The complexes formed with a zinc atom at their metallic center may assume three different geometries: trigonal, octahedral, and tetrahedral, the latter being the most common geometry for zinc complexes described in the literature^{13,14}. The second most abundant metal ion in the human body after Fe²⁺, Zn²⁺ is considered a biometal as it plays a vital role in regulating metalloenzymes, which act as structural and catalytic cofactors¹⁵. The human body has higher

*Corresponding author: Andréa L. F. de Souza

Email address: andrealuzia@gmail.com

DOI: <http://dx.doi.org/10.13171/mjc02303071666souza>

Received December 9, 2022

Accepted January 8, 2023

Published March 7, 2023

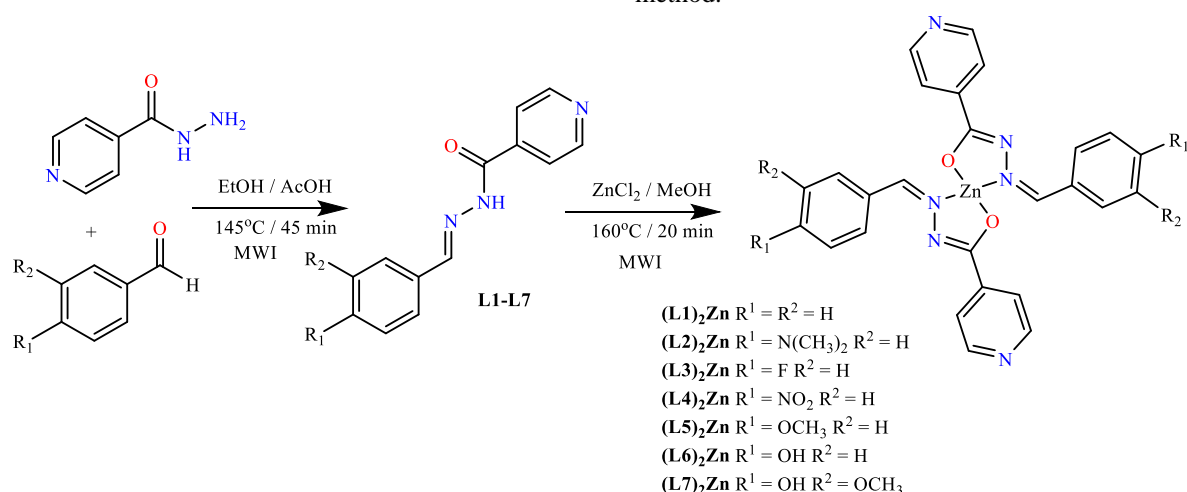
concentrations of Zn^{2+} in the brain. As we age, systemic zinc decreases, thereby promoting ion retention in the brain. The homeostatic deregulation of zinc leads to mitochondrial dysfunction and oxidative stress, two factors behind the development of neurodegenerative diseases, such as Alzheimer's and Parkinson's disease¹⁶.

It is well known that antioxidants inhibit the generation of reactive oxygen species (ROS) and the subsequent formation of lipid peroxidation products, thereby preventing oxidative stress. For instance, the accumulation of redox-active metal ions, such as Cu(I) and Cu(II), is responsible for increasing the concentration of toxic ROS. On the other hand, redox-inactive Zn(II) ions generally interact with amyloid-proteins (A), inducing their aggregation and forming of A β plaques. Both ROS and A β aggregates are thought to contribute to brain neurodegeneration¹⁷.

N-acylhydrazones complexes have been reported as having critical biological properties, such as antibacterial activity^{18–22}. According to the World Health Organization (WHO), bacterial resistance is a global threat to public health. Among pathogenic bacteria, *Staphylococcus aureus* is the cause of many infections, such as those isolated in the community

and healthcare-associated conditions. In addition, bacteremia, urinary tract infections, and skin infections are caused by methicillin-resistant *S. aureus* (MRSA)^{23–25}. Therefore, searching for new compounds that inhibit MRSA bacteria is very important.

This study presents the synthesis through microwave assisted-condensation and characterization of isoniazid-based *N*-acylhydrazone ligands (**L1–L7**). Microwave irradiation was also employed to synthesize Zn(II) complexes from **L1–L7** ligands (Scheme 1) under fixed suitable conditions, which was highly efficient. This high synthetic efficiency is due to several advantages of microwave-assisted (MW) synthesis advantages) can make the reaction faster, economical, safer, more reactive, reproducible, with a higher yield, and environmentally sustainable. This is because of its efficient heating from the rapid oscillation of the molecule's dipole through microwaves, resulting in dielectric heating and uniform heat distribution in the reaction medium^{26–31}. In this way, seven Zn(II) complexes were synthesized, and their structures and stability were determined by spectroscopy and DFT. Its antioxidant activity was evaluated by the DPPH method.



Scheme 1. Microwave-assisted synthesis of Zn(II) complexes from derivatives **L1–L7**.

2. Results and Discussion

2.1. Synthesis of Zn(II)-*N*-acylhydrazone derivative complexes

The *N*-acylhydrazones **L1–L7** (**L** = Hydrazone ligand) compounds were synthesized by Schiff base condensation of isoniazid (isonicotinic acid hydrazide - INH) and respective aldehyde under microwave irradiation (MWI) in high yield according to our previous study¹⁸. Reactions carried out under MI are favored by our research group due to some advantages over conventional conditions, such as shorter reaction time. The microwave assisted-synthesis between two equivalents of **L1–L7** ligands with one equivalent of anhydrous zinc dichloride in MeOH produced Zn(II) complexes in good yields (outline Scheme 1). HMRS (Figures S1–7) confirmed the percent values

calculated and suggested a 1:2 metal: ligand stoichiometric ratio for all synthesized complexes. Zn(II) is four coordinated by two carbonyls and two imine molecules from two *N*-acylhydrazones ligands. All ligands are soluble in methanol, dimethyl sulfoxide (DMSO), and chloroform and partially soluble in ethanol. All complexes were insoluble in water, sparingly in dichloromethane and acetone, and soluble in methanol and DMSO. In addition, all compounds are stable in the respective mentioned solvents, observed by the non-change of color and the wavelength displacement from the solution UV-vis, which will be discussed in topic 2.5.

2.2. Thermal analysis

Thermogravimetric analysis (TGA) was conducted for *N*-acylhydrazones and Zn(II) complexes from 30

to 800°C under nitrogen flow to investigate their stability. The results are shown in Figure 1, whereas Table 1 shows the molecules' decomposition stages, temperature ranges, and calculated weight loss percentages. Analyses (TGA and DTG curves) of the ligands and corresponding complexes are found in the supplemental material (Figures S8-14).

Most ligands show a one-stage decomposition pattern. The L2, L3, and L5 ligands exhibited one more decomposition stage with 5% of weight assignment to solvent loss. The results show that all complexes have a similar 3-step decomposition pattern. The first stage is attributed to eliminating water or solvent, the second to losing one mol of the ligand, and the third

to remove the remaining ligand, leaving behind ZnO as residue. No weight loss indicates the presence of coordinated water molecules in these complexes. Given that, the proposed ligand: zinc stoichiometry ratio is 2:1³².

The thermal stability profile of ligands and metal complexes depends on the nature of the substituents consistent with electron donor or withdrawing reactivity. That was observed at the onset temperature of the second decomposition stage of the complexes. In ascending order, L3 and (L3)₂Zn exhibited the lowest thermal stability whereas L6, L7, (L6)₂Zn and (L7)₂Zn were the most stable molecules.

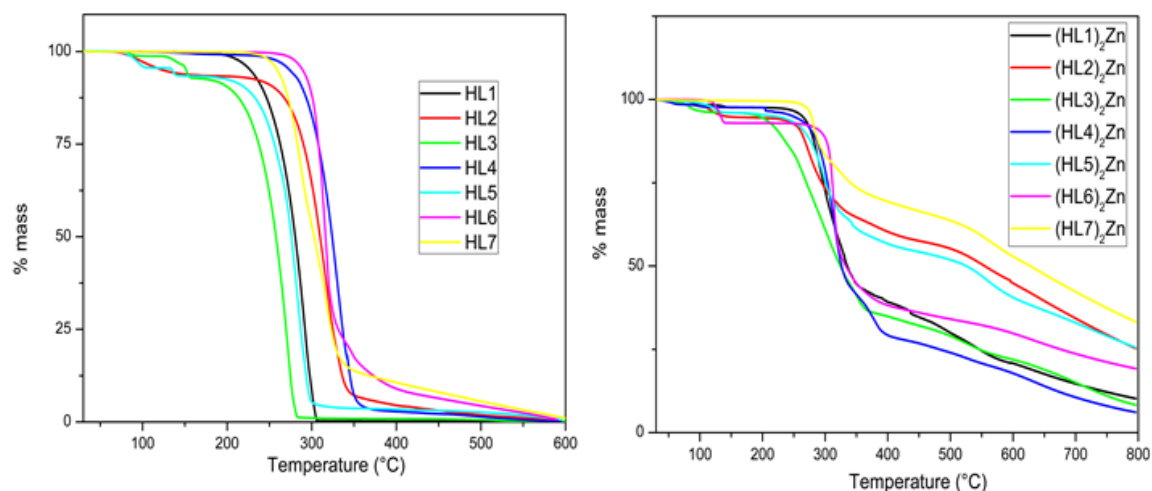


Figure 1. TGA spectrum of L1-7 compounds and corresponding Zn(II) complexes.

Compounds (F. wt)	DTG (max) (°C)	Decomposition Temperature Range (°C)	Weight loss found (calculated %)	Decomposition assignment
L1	291	176.2 - 307.4	100	Degradation of ligand
(L1) ₂ Zn	292	71.4 - 143.3	2.43	Loss of water
		231.9 - 370.3	54.95	Loss of ligand
		370.3 - 795.7	32.73	Formation of ZnO
L2	315	71.5 - 147.6	6.13	Loss of solvent
		216.0 - 593.4	93.87	Degradation of ligand
(L2) ₂ Zn	273	90.4 - 162.3	5.3	Loss of water
		225.9 - 442.3	35.9	Loss of ligand
		442.4 - 795.3	32.15	Formation of ZnO
HL3	271	67.6 - 158.7	7.13	Loss of solvent
		169.6 - 288.6	92.87	Degradation of ligand
(HL3) ₂ Zn	301	65.6 - 105.8	3.56	Loss of water
		172.4 - 380.8	60.1	Loss of ligand
		380.8 - 791.4	27.04	Formation of ZnO

L4	330	232.7 - 517.2	100	Degradation of ligand
(L4)₂Zn	314	39.1 - 111.0	2.43	Loss of water
		221.0 - 351.5	54.69	Loss of ligand
		351.5 - 778.1	34.74	Formation of ZnO
L5	282	75.8 - 146.3	6.42	Loss of solvent
		188.8 - 332.5	93.58	Degradation of ligand
(L5)₂Zn	297	93.3 - 138.8	3.85	Loss of water
		215.2 - 438.0	40.72	Loss of ligand
		438.0 - 795.7	28.75	Formation of ZnO
L6	312	247.3 - 552.3	100	Degradation of ligand
(L6)₂Zn	312	113.9 - 143.3	7.26	Loss of water
		266.4 - 483.4	58.11	Loss of ligand
		483.4 - 798.6	15.38	Formation of ZnO
L7	287	235.5 - 618.4	100	Degradation of ligand
(L7)₂Zn	282	251.8 - 423.3	32.05	Loss of ligand
		423.3 - 794.3	34.73	Formation of ZnO

Table 1. Thermal analysis data of *N*-acylhydrazone ligands and corresponding complexes.

2.3. Powder XRD studies

Powder X-ray diffraction (XRD) analysis was performed for the Zn(II) complexes to determine their crystalline nature. Diffractograms (Figures S15-21) indicate that the complexes have structural regularity, *i.e.*, they are in their crystalline morphology³²⁻³⁴. Since one trend of the peaks from maximum to minimum intensity, it is proposed that the samples were mainly ordered³⁴. The Bragg law and Debye-

Scherrer equation 35 defined the complexes' basal spacing and crystallite dimensions. The data shown in Table 2 indicate that their crystalline dimensions range from 32 to 86 nm. The calculated crystallite size suggests that the *N*-acylhydrazones complex are in the nanocrystalline phase. This behavior agrees with some complex characterizations reported in the literature³²⁻³⁴.

Table 2. The powder XRD data of Zn(II) complexes.

Complex	2 θ	d-spacing (Å)	FWHM: β (10^{-3})	Crystallite Size (nm)
(L1)₂Zn	6.07	4.08	3.05	50.59
(L2)₂Zn	23.28	15.53	4.75	33.12
(L3)₂Zn	14.67	9.78	4.74	32.78
(L4)₂Zn	42.86	28.11	1.91	86.70
(L5)₂Zn	25.25	16.79	2.44	64.73
(L6)₂Zn	5.96	3.93	3.02	51.10
(L7)₂Zn	9.45	6.31	3.51	44.05

2.4. IR spectra

Infrared (IR) spectra of *N*-acylhydrazone ligands and corresponding zinc complexes were analyzed in the 4000-400 cm^{-1} region (Figures S22-S35). Table 3 shows the infrared data for ligands and corresponding Zn(II) complexes. The complex formation and structure were deduced by comparing vibrational spectra data of free ligand and metal complexes. The azomethine (C=N), carbonyl (C=O), and amine (NH) groups stretching vibrations were followed to show

their involvement in chelation with zinc. Theoretical and experimental data were used to establish the band's correlation.

The band at 3224-3587 cm^{-1} range in the IR spectrum of *N*-acylhydrazones (L1-7) is attributed to the vibration of the NH group. As per the experimental and theoretical calculations, $\nu(\text{NH})$ mode in the 3485-3517 cm^{-1} region shifted to 3574-3584 cm^{-1} for the Zn(II) complexes. In the same sense, $\nu(\text{C=O})$ bands at 1654-1687 cm^{-1} in the spectra of free *N*-

acylhydrazones shifted to 1656-1681 cm^{-1} range in the spectra of the complexes, suggesting coordination through the nitrogen and oxygen atoms³⁶⁻³⁹.

The theoretical calculations predicted $\nu(\text{C}=\text{O})$ bands at 1808-1833 cm^{-1} and 1593-1619 cm^{-1} for the free ligands and Zn(II) complexes. Since frequencies calculated in this region are overestimated, scaling factors are usually used; however, as we were only interested in the vibrational assignment, not in the exact reproduction of the vibrational frequencies, no scaling factor was employed. However, in both theoretical and experimental data, the decrease in the lowest wave number of the $\nu(\text{C}=\text{O})$ band indicates the weakening of C=O bonds, the formation of Zn-OC bonds, and the formation of Zn(II) complexes.

The characteristic absorption band at 1560-1602 cm^{-1} is due to azomethine linkage⁴⁰, which suggests successful condensation and formation of the *N*-acylhydrazone ligand. Also, the azomethine linkage band of the ligand shifted to different frequencies (1565-1608 cm^{-1}), possibly due to zinc ion complexation via azomethine nitrogen⁴¹.

A theoretically weak transition assigned to the (C=N) mode for the free ligands can be observed in 1694-1716 cm^{-1} . This band shift to 1589-1606 cm^{-1} for the Zn(II) complexes indicates the formation of Zn-NC bonds. Furthermore, new weak bands appeared at lower frequencies at 426-454 cm^{-1} , associated with metal to nitrogen^{42,43}. A weak transition corresponding to $\nu(\text{Zn}-\text{N})$ was also predicted in the 479-518 cm^{-1} . These theoretical frequencies are shown in Table S1.

Table 3. IR spectral data of the *N*-acylhydrazones and corresponding Zn(II) complexes.

Compound	$\nu(\text{NH})$	$\nu(\text{C}=\text{O})$	$\nu(\text{C}=\text{C})$	$\nu(\text{C}=\text{N})$	$\nu(\text{M}-\text{N})$
L1	3450	1687	1602	1562	-
L2	3404	1664	1595	1523	-
L3	3469	1656	1598,1558	1506	-
L4	3439	1685	1562	1508	-
L5	3439	1656	1602	1510	-
L6	3224	1658	1597	1552	-
L7	3417	1654	1575	1516	-
(L1)₂Zn	3450	1666	1608	1554	449
(L2)₂Zn	3441	1660	1600	1533	426
(L3)₂Zn	3585	1681	1606	1504	454
(L4)₂Zn	3587	1681	1560	1510	451
(L5)₂Zn	3431	1674	1602	1510	438
(L6)₂Zn	3429	1656	1597,1552	1510	449
(L7)₂Zn	3363	1660	1593,1556	1536	441

Therefore, the geometry of the complexes appears to be consistent with the tetradentate coordination of *N*-acylhydrazone derivatives through the carbonyl oxygen and azomethine nitrogen (Figure 2). DFT calculations predicted Zn-N and Zn-O bond lengths of 2.04–2.07 Å and 1.98–2.04 Å, respectively (Tables S1-S3). These values agree with X-ray data reported for similar Zn(II) complexes, which were found to be 2.01 Å and 1.91 Å, respectively⁴³⁻⁴⁵.

2.5 UV-Vis data

UV/vis absorption spectra of the Zn(II) complexes and corresponding free ligands (Figure S36-42) were measured in methanolic solution at room temperature in the 200–600 nm range. The results are presented in Figure 3 and Table 4.

Zn(II) ions in these complexes have a d^{10} configuration; therefore, they do not show any absorption in the visible region corresponding to d-d transitions.

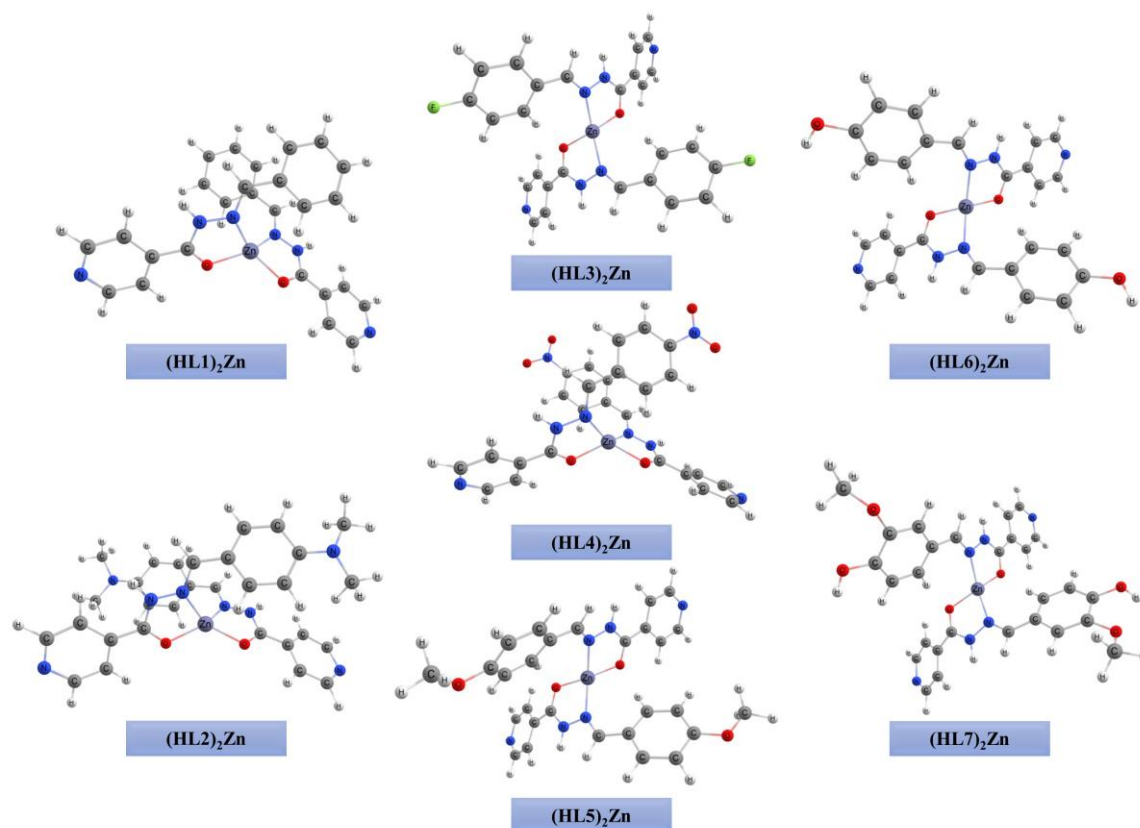


Figure 2. Calculated structure for complexes $(\text{HL1})_2\text{Zn}$ – $(\text{HL7})_2\text{Zn}$ at B3LYP/def2-SVP level.

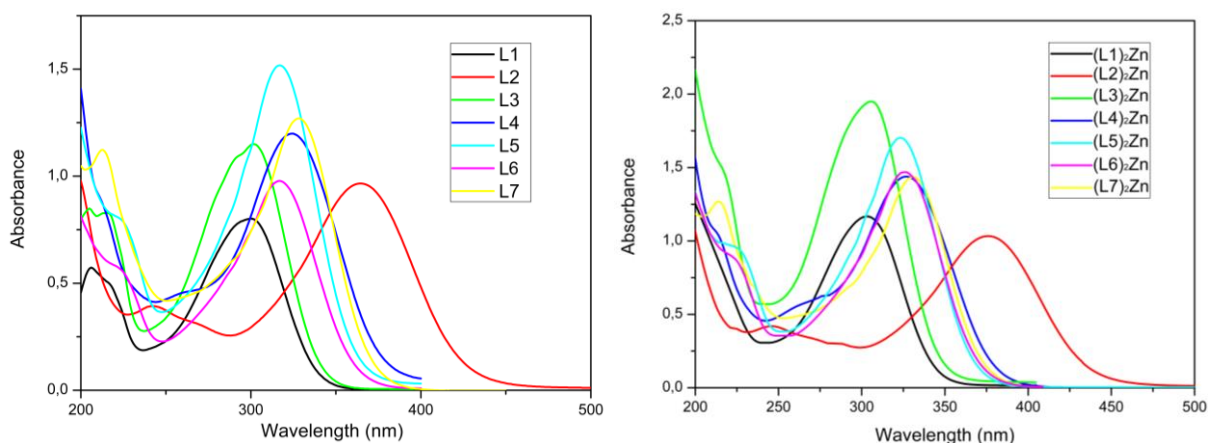


Figure 3. UV-Vis spectrum (MeOH) of **L1-7** compounds and corresponding Zn(II) complexes.

The Absorption spectra of the Zn(II) complexes and free ligands is characterized by two main absorption bands in the region 275–5000 nm. The bands at higher energy are ascribed to $\pi \rightarrow \pi^*$ transitions of the aromatic system of the compounds. The bands at lower energy ($\epsilon = 48000\text{--}80000 \text{ L mol}^{-1} \text{ cm}^{-1}$ range) can be attributed to the $n \rightarrow \pi^*$ transitions of C=N and C=O groups. By comparing the behavior of the free ligands to corresponding complexes, it is possible to observe a red shift in absorption spectra. This shift indicates that the introduction of the Zn(II) ion

enlarged the ligand's conjugated system, which suggests that the nitrogen atom of the C=N group and the oxygen atom of the C=O group of ligands are coordinated successfully to the central Zn(II) ion ⁴⁶.

2.6. Electrochemical Properties

To clarify the relative contributions of the substituent groups to the redox character of *N*-acylhydrazones, cyclic voltammetry (-1.0 V to 1.0 V) was performed for the seven Zn(II) complexes, i.e., $(\text{L1})_2\text{Zn}$ to $(\text{L7})_2\text{Zn}$, at $1.0 \times 10^{-3} \text{ mol L}^{-1}$ in DMSO. Figure 4 shows the cyclic voltammograms of the Zn(II) complexes.

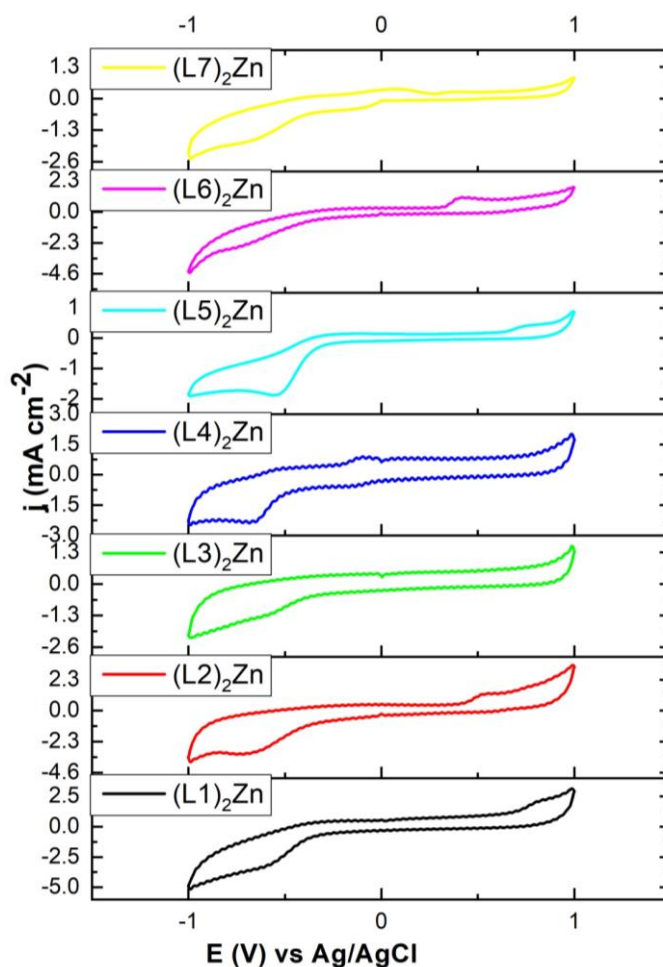
Table 4. UV data of *N*-acylhydrazones and Zn(II) complexes.

Ligand	λ_{\max} (nm)	Complex	λ_{\max} (nm)
L1	298.10	(L1) ₂ Zn	302.68
L2	364.39	(L2) ₂ Zn	375.49
L3	300.68	(L3) ₂ Zn	305.20
L4	324.11	(L4) ₂ Zn	326.54
L5	316.69	(L5) ₂ Zn	323.26
L6	316.95	(L6) ₂ Zn	325.38
L7	327.53	(L7) ₂ Zn	331.24

The cyclic voltammograms of Zn(II) complexes (-1.0V to 1.0V) were characterized by a reversible redox process for (L4)₂Zn, and an irreversible (both cathodic and anodic) method for the remaining six complexes (L1)₂Zn-(L3)₂Zn and (L5)₂Zn - (L7)₂Zn. Voltammetry curves of complex (L4)₂Zn were characterized by one reversible redox process at -0.07/-0.15 V, ($E_{1/2} = -0.11$) vs. Ag⁺/AgCl, which was assigned to the nitro group, previously reported for other aromatic derivatives⁴⁷. The remaining six complexes exhibit two irreversible (cathodic and

anodic) processes. The irreversible reduction process at -0.70 V is attributed to the Zn(II)/Zn center in (HL)₂Zn. This value agrees with those reported for related Zn Schiff base complexes⁴⁸.

The different values for the oxidation and reduction processes are probably related to the presence of the electron-donor [OH, N(CH₃)₂] or electron-withdrawing [NO₂, F] substituent groups in *N*-acylhydrazones.

**Figure 4.** Cyclic voltammogram of the Zn(II) complexes (DMSO, KCl, scan rate 50 mV s⁻¹).

The experimental values of the highest occupied molecular orbital (HOMO) energy levels and lowest

unoccupied molecular orbital (LUMO) energy levels of Zn(II) complexes were obtained according to

electrochemical parameters and electronic spectra^{49,50}. The HOMO and LUMO values were obtained using the equations: $E_{\text{HOMO}} = 4.74 + E_{\text{OX}}$; $E_{\text{LUMO}} = E_{\text{HOMO}} - E_{\text{g}}$, $E_{\text{g}} = 1240 / \lambda_{\text{onset}}$ (eV), where λ_{onset} is the highest absorption band⁵¹. Table S3 shows both cathodic and anodic peak potentials for the first reduction (E_{pc1}) and oxidation (E_{pa1}) steps at a sweep rate of 50 mV s^{-1} and HOMO and LUMO values.

As shown in Table 5, the oxidation potential and the HOMO energy level of the complexes with the

electron-donor group are higher than those without a substituent. In contrast, the oxidation potential and HOMO energy level of the complex with an electron-withdrawing group are lower than those without a substituent. The frontier orbital theory⁵² can explain the above phenomena; the HOMO prioritizes providing electrons.

For electron donor compounds, the oxidation process corresponds to losing electrons in HOMO.

Table 5. The Zn(II) complexes E_{red} , E_{ox} , E_{HOMO} , E_{LUMO} , and E_{g} .

Complex	E_{red}	E_{ox}	E_{g}	E_{HOMO}	E_{LUMO}
(HL1) ₂ Zn	-0.56	0.81	4.09	5.55	1.45
(HL2) ₂ Zn	-0.65	0.54	3.30	5.28	1.97
(HL3) ₂ Zn	-0.57	0.21	4.06	4.95	0.86
(HL4) ₂ Zn	-0.15	-0.07	3.79	4.67	0.87
(HL5) ₂ Zn	-0.53	0.75	3.83	5.49	1.65
(HL6) ₂ Zn	-0.58	0.43	3.81	5.16	1.35
(HL7) ₂ Zn	-0.6	0.62	3.74	5.36	1.61

2.7 Antioxidant activity

In vitro antioxidant activity of synthesized *N*-acylhydrazones (L1-7) and Zn(II) complexes was assessed using DPPH (1,1-Diphenyl-2-picrylhydrazyl) stable free radicals and compared to that of ascorbic acid. DPPH radicals are the primary method for screening compounds capable of scavenging activated oxygen species because they are more stable and easier to handle than oxygen-free radicals. Consequently, DPPH assays have been widely used to assess the antioxidant activity of different compounds⁵³.

This method measures the continual absorbance decrease in the methanol solution of the stable free nitrogen radical DPPH at 517 nm in the presence of the compounds tested^{54,55}. All tested *N*-acylhydrazones and their complexes exhibit UV

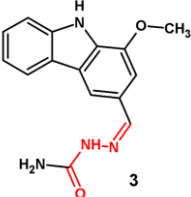
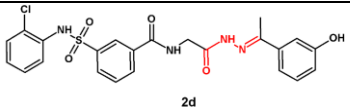
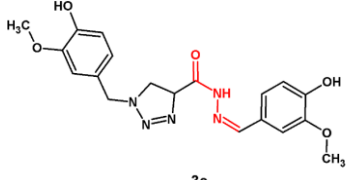
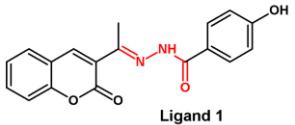
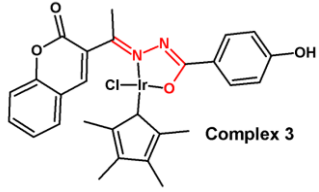
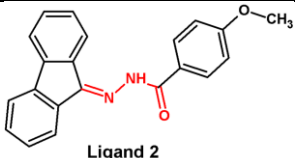
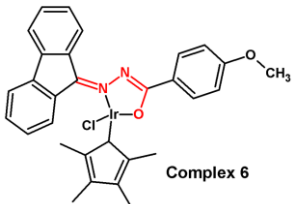
absorbance between 230 and 350 nm and do not interfere with the kinetic measurement of DPPH absorbance decrease at 517 nm. The DPPH• absorbance decrease in the presence of antioxidants is due to hydrogen transfer from the antioxidant, thus forming the DPPH-H stable compound. Methanolic DPPH• solutions used at different concentrations were stable (checked over 30 min).

The IC₅₀ values were determined for all compounds (Table 6). Compounds with a withdrawing group have the lowest IC₅₀ values among the synthesized *N*-acylhydrazones, best results for compounds L7 and (L7)₂Zn (65.3 and 78.7 $\mu\text{mol.l}^{-1}$, respectively). In addition, compounds L7 and (L7)₂Zn remain efficient compared to the antioxidant activity of other *N*-acylhydrazones synthesized in the literature, which use ascorbic acid as a standard (Table 7).

Table 6. Results of antioxidant activity by DPPH method.

Ligand	DPPH IC ₅₀ ($\mu\text{mol. l}^{-1}$)	Complex	DPPH IC ₅₀ ($\mu\text{mol. l}^{-1}$)
L1	532.74	(L1) ₂ Zn	429.04
L2	221.76	(L2) ₂ Zn	222.75
L3	465.04	(L3) ₂ Zn	432.63
L4	458.31	(L4) ₂ Zn	436.20
L5	243.40	(L5) ₂ Zn	267.56
L6	285.04	(L6) ₂ Zn	279.33
L7	65.30	(L7) ₂ Zn	78.70
Ascorbic acid	47.20		

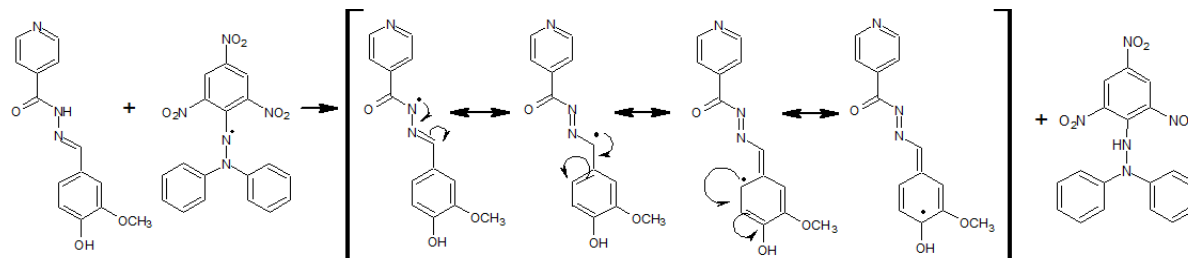
Table 7. Antioxidant activity results of some *N*-acylhydrazones derivatives from the literature with **HL7** and **(HL7)₂Zn**.

Compound	IC ₅₀	%DRSA*	Year	Ref
 3	7.3 μmol.l ⁻¹	-	2016	56
Ascorbic Acid	4.4 μmol.l ⁻¹	-		
 2d	25.3 μmol.l ⁻¹	-	2017	57
Ascorbic Acid	20.7 μmol.l ⁻¹	-		
 3e	30.4 mg.ml ⁻¹	-	2020	58
Ascorbic Acid	14.9 mg.ml ⁻¹	-		
 Ligand 1	-	39.7		
 Complex 3	-	85.0	2021	59
Ascorbic Acid	-	99.0		
 Ligand 2	-	22.7		
 Complex 6	-	67.6	2022	60
Ascorbic Acid	-	95.3		
HL7	65.30 μmol.l ⁻¹	-		
(HL7)₂Zn	78.70 μmol.l ⁻¹	-	2023	This Work
Ascorbic Acid	45.20 μmol.l ⁻¹	-		

*DPPH radical scavenging activity

According to the literature^{55,61}, the hydrogen atom of the isoniazid moiety in a position from the hydrazone function is highly activated. *N*-acylhydrazone may easily undergo the abstraction of one hydrogen atom from this position. Hydrazones possessing at least one hydrogen atom on nitrogen, the formation of

N^{\bullet} radical, which is stabilized through conjugation, forming delocalized C^{\bullet} radicals (Scheme 2). The different DPPH $^{\bullet}$ scavenging properties (IC_{50}) of the hydrazone ligands and their complexes may reflect the relative ability to abstract of the N-H hydrogen atom from the compound in question.



Scheme 2. Purposed reaction of DPPH $^{\bullet}$ with L7⁶¹.

3. Conclusion

In summary, seven Zn(II) complexes containing *N*-acylhydrazone ligands (L1-7) were prepared by microwave irradiation and characterized by HRMS, UV-Vis, and IR spectroscopy. Theoretical calculations suggested a tetrahedral geometry for the Zn(II) complexes, with the metal coordinating with the OC and NC regions of the ligands. Based on the thermal data, we conclude that the complexes (L6)₂Zn and (L7)₂Zn are the most stable. Voltammetry curves of (L4)₂Zn indicated one reversible redox process at -0.07/-0.15 V, ($E_{1/2} = -0.11$) vs.

Ag+/AgCl, which was assigned to the nitro group. The different values for the oxidation and reduction processes are probably related to the presence of the electron-donor [OH, N(CH₃)₂] or electron-withdrawing [NO₂, F] substituent groups in *N*-acylhydrazones. In addition, the oxidation potential and the HOMO energy level of the complexes with the electron donor group ($E_{HOMO} = 5.49 - 5.16$ eV) are higher than those of the complex with electron acceptor groups ($E_{HOMO} = 4.95 - 4.97$ eV). The antioxidant activity assays showed that L7 ($IC_{50} = 65.30$ $\mu\text{mol}\cdot\text{l}^{-1}$) and its complex (L7)₂Zn ($IC_{50} = 78,70$ $\mu\text{mol}\cdot\text{l}^{-1}$) were the most active substances compared to standard ascorbic ($IC_{50} = 47.20$ $\mu\text{mol}\cdot\text{l}^{-1}$).

Acknowledgments

The authors would like to thank the Farmanguinhos-FIOCRUZ for the HRMS spectra data, Programa de Pós-Graduação em Ciência e Tecnologia para Recursos Amazônicos (PPGCTRA – UFAM), Fundação de Amparo à Pesquisa do Estado do Amazonas – FAPEAM (process n°. 005/2019), PROPESP/UFAM-CNPq (process n°. 041/2016 and 008/2018), Fundação Carlos Chagas de Amparo à Pesquisa do Estado do Rio de Janeiro – FAPERJ (grant number E-26/210.070/2022; SEI-260003/015957/2021; SEI-260003/015018/2021-

APQ1 and E-26/201.248/2022 –SEI-260003/003411/2022–BBP), and Coordenação de Aperfeiçoamento de Pessoal de Nível Superior Brazil (CAPES) and Conselho Nacional de Desenvolvimento Científico – CNPq for financial support.

4. Experimental

All chemicals and solvents were used as received. All aldehydes are Sigma-Aldrich®; zinc chloride anhydrous, MeOH, and EtOH are Neon®, CH₂Cl₂ is Vetec®, and isoniazid is Merck®. All reactions were performed under microwave irradiation with Anton Paar® Monowave 300. Fisatom® (Brazil) recorded all synthesized compounds' melting points. UV/Vis analyses were recorded on Shimadzu® (UV2600) using DMSO as solvent. Infrared spectra of the synthesized ligands and Zn(II) complexes were recorded on FT-IR Shimadzu® (IFAffinity-1) with KBr pellets within the 400-4000 cm^{-1} range. All thermogravimetric analyses (TGA) were performed using a TA Instruments® analyzer (TGA Q50) under nitrogen gas flow (60 mL/min) at 10°C min⁻¹ heating rate from room temperature (25°C) up to 800°C. Powder X-ray diffraction (XRD) studies were performed on a Rigaku® Ultima IV X-ray diffractometer (CuK α irradiation, 40 kV, 20 mA) in the range of 1.5-80° 2 θ . Electrochemical analyses were recorded on an Autolab® potentiostat/galvanostat by cyclic voltammetry curve testing with the glassy electrode (0.07 cm^2) as work electrode, a platinum plate electrode (1 cm^2) as a counter electrode, and an Ag/AgCl as a reference electrode. KCl solution was used as a supporting electrolyte and DMSO as solvent. The electrolytes were degassed with pure argon gas, and the test scanning speed was 50 $\text{mV}\cdot\text{s}^{-1}$.

4.1. Microwave assisted-synthesis of Zn(II) Complexes

L1-L7 ligands (1 mmol) and zinc dichloride anhydrous (0.5 mmol) were dissolved in MeOH

(6 mL) in 10 mL vials. The solutions were stirred (1000 rpm) under microwave irradiation at 160°C for 20 min. The products were filtered off, washed with MeOH, and dried in air. Recrystallization with MeOH or CH₂Cl₂: MeOH produced the following pure zinc complexes:

- **(L1)₂Zn**: white solid; yield 74%; mp 284-285°C; UV-Vis (MeOH) λ/nm 302; IR (KBr) ν/cm⁻¹ 3450, 3242, 3037, 2922, 2854, 1666, 1608, 1554, 1294, 1060, 696, 511, 449; HRMS (FTMS + pESI) *m/z* observed 514.8639; C₂₆H₂₁N₆O₂Zn [M]⁺ expected: 514.8639.
- **(L2)₂Zn**: orange solid; yield 83%; mp 244-246°C; UV-Vis (MeOH) λ/nm 375; IR (KBr) ν/cm⁻¹ 3441, 3045, 2924, 2856, 1660, 1600, 1533, 1367, 1305, 1180, 1062, 700, 503; HRMS (FTMS + pESI) *m/z* observed 599.1857; C₃₀H₃₁N₈O₂Zn [M]⁺ expected 600.9995.
- **(L3)₂Zn**: white solid; yield 73%.; mp 247-249°C; UV-Vis (MeOH) λ/nm 305; IR (KBr) ν/cm⁻¹ 3583, 3481, 3269, 3072, 2821, 1681, 1606, 1504, 1290, 1232, 1151, 1068, 840, 702, 532; HRMS (FTMS + pESI) *m/z* observed 549.0817; C₂₆H₁₉F₂N₆O₂Zn [M]⁺ expected 550.8448.
- **(HL4)₂Zn**: greenish yellow solid; yield 72%; mp 268-270°C; UV-Vis (MeOH) λ/nm 326; IR (KBr) ν/cm⁻¹ 3587, 3184, 3001, 2893, 2827, 1681, 1560, 1510, 1336, 1280, 1143, 1068, 842, 686, 503; HRMS (FTMS + pESI) *m/z* observed 603.0703; C₂₆H₁₉N₈O₆Zn [M]⁺ expected 604.8590.
- **(L5)₂Zn**: greenish yellow solid; yield: 93%; mp 248-250°C; UV-Vis (MeOH) λ/nm 323; IR (KBr) ν/cm⁻¹ 3693, 3431, 3223, 3043, 2833, 1674, 1602, 1510, 1301, 1253, 1170, 1028, 833, 696, 522; HRMS (FTMS + pESI) *m/z* observed 573.1195; C₂₈H₂₅N₆O₄Zn [M]⁺ expected 574.9159.
- **(L6)₂Zn**: orange-yellow solid; yield 74%; mp 283-285°C; UV-Vis (MeOH) λ/nm 325; IR (KBr) ν/cm⁻¹ 3429, 3221, 3028, 1656, 1597, 1552, 1510, 1286, 1226, 1159, 1058, 831, 688, 607, 526; HRMS (FTMS + pESI) *m/z* observed: 546.8627; C₂₆H₂₁N₆O₄Zn [M]⁺ expected 546.8627.
- **(HL7)₂Zn**: dark yellow solid; yield 82%; mp 244-246°C; UV-Vis (MeOH) λ/nm 331; IR (KBr) ν/cm⁻¹ 3363, 3250, 2922, 1660, 1593, 1556, 1517, 1384, 1292, 1134, 1029, 698, 599, 441; HRMS (FTMS + pESI) *m/z* observed 605.1123; C₂₈H₂₅N₆O₆Zn [M]⁺ expected 606.9147.

4.2. Theoretical calculations

Quantum chemical calculations using Density Functional Theory (DFT) were performed to predict the structures and spectroscopic properties of the Zn(II) complexes. The geometries for the ligands and Zn(II) complexes were optimized in the gas phase at the B3LYP level with the def2-SVP basis set for all atoms. The same level of theory was used to calculate the vibrational frequencies to characterize the structures as true minima on the potential energy surface (all real harmonic frequencies) and to analyze the normal vibrational modes. All calculations were done using the ORCA 4.1.1 program (Neese 2012).

4.3. DPPH radical scavenging assay

All the tested compounds were dissolved in methanol. Then, 0.1 mL of each was added (0 - blank control, 100, 200, 500, and 1000 μmol/L) to 3.9 mL of DPPH (0,005 % (w/v)) and incubated at room temperature for 1 h.

Absorbance was measured at 517 nm (Santos et al. 2020), and the half maximal inhibitory concentration (IC₅₀) was calculated by plotting a non-linear regression % inhibition vs. concentration curve with Origin software (version 8.1). Ascorbic acid was employed as a positive control. The % inhibition was expressed as a percentage of scavenging activity on DPPH: SC% = [(A_{control} - A_{test})/A_{control}]. · 100%, where A_{control} and A_{test} are the absorbances of the control (DPPH solution without test sample) and the test sample (DPPH solution plus scavenger), respectively. The control contains all reagents except the scavenger.

Supplementary data

Electronic Supplementary material associated with this article can be found in the online version of this paper.

References

- 1- D. G. Guimarães, L. A. Rolim, A. de A. Gonsalves, C. R. M. Araújo, Investigação do Potencial Bilógico de Hidrazonas Obtidas Sinteticamente na Última Década (2006-2016): Uma Revisão Sistemática, *Revista Virtual de Química*, **2017**, 9, 2551–2592.
- 2- A. Kajal, S. Bala, N. Sharma, S. Kamboj, V. Saini, Therapeutic Potential of Hydrazones as Anti-Inflammatory Agents, *Int J Med Chem*, **2014**, 2014, 1–11.
- 3- P. G. Cozzi, Metal-Salen Schiff base complexes in catalysis: Practical aspects, *Chem Soc Rev*, **2004**, 33, 410–421.
- 4- R. Manikandan, P. Viswanathamurthi, M. Muthukumar, Ruthenium(II) hydrazone Schiff base complexes: Synthesis, spectral study and catalytic applications, *Spectrochim Acta A Mol Biomol Spectrosc*, **2011**, 83, 297–303.

- 5- E. M. Barbosa, K. S. Souza, P. H. S. de Oliveira, Í. S. Costa, I. V. de França, L. dos Santos Mello, E. R. Dockal, J. da Cruz, E. A. Souza, P. J. S. Maia, Uranyl Salen-Type Complex as Co-catalyst for Electrocatalytic Oxidation of Ethanol, *Electrocatalysis*, **2021** doi:10.1007/s12678-021-00697-0.
- 6- R. D. dos Santos, S. de Fatima Freire dos Santos, F. da Silva Moura, P. J. S. Maia, B. T. da Fonseca, R. H. de Almeida Santos, M. E. Medeiros, F. M. dos Santos Garrido, A. Casellato, A nickel(II) coordination polymer derived from a tridentate Schiff base ligand with N, O-donor groups: synthesis, crystal structure, spectroscopy, electrochemical behavior and electrocatalytic activity for H₂O₂ electroreduction in alkaline medium, *Transition Metal Chemistry*, **2017**, 42, 301–310.
- 7- H. Kargar, M. Fallah-Mehrjardi, R. Behjatmanesh-Ardakani, K. S. Munawar, M. Ashfaq, M. N. Tahir, Synthesis, spectral characterization, SC-XRD, HSA, DFT and catalytic activity of a dioxidomolybdenum complex with aminosalicyl-hydrazone Schiff base ligand: An experimental and theoretical approach, *Polyhedron*, **2021**, 208 doi:10.1016/j.poly.2021.115428.
- 8- H. Kargar, M. Fallah-Mehrjardi, R. Behjatmanesh-Ardakani, K. S. Munawar, M. Ashfaq, M. N. Tahir, Synthesis, spectral characterization, SC-XRD, HSA, DFT and catalytic activity of novel dioxovanadium(V) complex with aminobenzohydrazone Schiff base ligand: An experimental and theoretical approach, *Inorganica Chim Acta*, **2021**, 526 doi:10.1016/j.ica.2021.120535.
- 9- H. Kargar, M. Fallah-Mehrjardi, R. Behjatmanesh-Ardakani, K. S. Munawar, M. Ashfaq, M. N. Tahir, Diverse coordination of isoniazid hydrazone Schiff base ligand towards iron(III): Synthesis, characterization, SC-XRD, HSA, QTAIM, MEP, NCI, NBO and DFT study, *J Mol Struct*, **2022**, 1250 doi:10.1016/j.molstruc.2021.131691.
- 10- H. Kargar, M. Fallah-Mehrjardi, R. Behjatmanesh-Ardakani, K. S. Munawar, M. Ashfaq, M. N. Tahir, Titanium(IV) complex containing ONO-tridentate Schiff base ligand: Synthesis, crystal structure determination, Hirshfeld surface analysis, spectral characterization, theoretical and computational studies, *J Mol Struct*, **2021**, 1241 doi:10.1016/j.molstruc.2021.130653.
- 11- H. Kargar, M. Nateghi-Jahromi, M. Fallah-Mehrjardi, R. Behjatmanesh-Ardakani, K. S. Munawar, S. Ali, M. Ashfaq, M. N. Tahir, Synthesis, spectral characterization, crystal structure and catalytic activity of a novel dioxomolybdenum Schiff base complex containing 4-aminobenzhydrazone ligand: A combined experimental and theoretical study, *J Mol Struct*, **2022**, 1249 doi:10.1016/j.molstruc.2021.131645.
- 12- H. Kargar, M. Fallah-Mehrjardi, R. Behjatmanesh-Ardakani, K. S. Munawar, Synthesis, spectra (FT-IR, NMR) investigations, DFT, FMO, MEP, NBO analysis and catalytic activity of MoO₂(VI) complex with ONO tridentate hydrazone Schiff base ligand, *J Mol Struct*, **2021**, 1245 doi:10.1016/j.molstruc.2021.131259.
- 13- E. S. Aazam, M. M. Ghoneim, M. A. El-Attar, Synthesis, characterization, electrochemical behavior, and biological activity of bis azomethine dye derived from 2,3-diaminomaleonitrile and 2-hydroxy-1-naphthaldehyde and its zinc complex, *J Coord Chem*, **2011**, 64, 2506–2520.
- 14- D. C. Santos, P. J. S. Maia, M. A. de Abreu Lopes, J. S. B. Forero, A. L. F. de Souza, A Simple Isoniazid-Based N-Acylhydrazone Derivative as Potential Fluorogenic Probe for Zn²⁺ Ions, *J Fluoresc*, **2021**, 31, 175–184.
- 15- Â. de Fátima, C. de P. Pereira, C. R. S. D. G. Olímpio, B. G. de Freitas Oliveira, L. L. Franco, P. H. C. da Silva, Schiff bases and their metal complexes as urease inhibitors – A brief review, *J Adv Res*, **2018**, 13, 113–126.
- 16- J. A. Duce, A. I. Bush, Biological metals and Alzheimer's disease: Implications for therapeutics and diagnostics, *Prog Neurobiol*, **2010**, 92, 1–18.
- 17- A. De Falco, D. S. Cukierman, R. A. Hauser-Davis, N. A. Rey, Doença de Alzheimer: Hipóteses etiológicas e perspectivas de tratamento, *Quim Nova*, **2016**, 39, 63–80.
- 18- D. C. Santos, R. R. Henriques, M. A. de A. L. Junior, A. B. Farias, T. L. do C. Nogueira, J. V. F. Quimas, N. C. Romeiro, L. L. da Silva, A. L. F. de Souza, Acylhydrazones as isoniazid derivatives with multi-target profiles for the treatment of Alzheimer's disease: Radical scavenging, myeloperoxidase/acetylcholinesterase inhibition and biometal chelation, *Bioorg Med Chem*, **2020**, 28 doi:10.1016/j.bmc.2020.115470.
- 19- L. L. Tevez, M. S. Islas, M. J. J. Medina, M. Diez, O. E. Piros, E. C. Eduardo, E. G. Ferrer, P. A. M. Williams, Structural, spectral and potentiometric characterization, and antimicrobial activity studies of [Zn(phen)₂(change)(H₂O)](NO₃)₂.H₂O, *J Coord Chem*, **2012**, 65, 2304–2318.
- 20- M. Almáši, Z. Vargová, D. Sabolová, J. Kudláčová, D. Hudecová, J. Kuchár, K. Györyová, Z. Vargová, D. Sabolová, J. Kudláčová, D. Hudecová, Ag (I) and Zn (II) isonicotinate complexes : design, characterization, antimicrobial effect, and CT-DNA binding studies, *J Coord Chem*, **2015**, 68, 4423–4443.
- 21- M. Poyraz, M. Sari, A. Guney, F. Demircis,

- S. Demirayak, E. Sahin, Synthesis, characterization and antimicrobial activity of a Zn (II) complex with 1- (1H- benzoimidazol-2-yl) -ethanone thiosemicarbazone, *J Coord Chem*, **2008**, 61, 3276–3283.
- 22-M. Amirnasr, R. S. Erami, K. Mereiter, K. S. Joß, S. Meghdadi, S. Abbasi, Syntheses, characterizations, X-ray crystal structures, and antibacterial activities of Co (II), Ni (II), and Zn (II) complexes of the Schiff base derived from 5-nitro-2-hydroxybenzaldehyde and benzylamine, *J Coord Chem*, **2015**, 68, 616–631.
- 23-I. C. R. L. Leal, K. R. N. Dos Santos, I. I. Júnior, O. A. C. Antunes, A. Porzel, L. Wessjohann, R. M. Kuster, Ceanothane and Lupane Type Triterpenes from *Zizyphus joazeiro* – An Anti-Staphylococcal Evaluation *, *Planta Med*, **2010**, 76, 47–52.
- 24-S. N. L. Aniele da, I. R. Guesdon, G. M. Corrêa, L. S. Silva, J. M. Mar, E. A. Sanches, A. B. Jaqueline de, D. F. de Moura do Carmo, Chemical composition and biological activities of the essential oil of *peumus boldus molina* (Monimiaceae), *Revista Virtual de Química*, **2020**, 12, 433–446.
- 25-A. T. Barbosa, V. H. N. da Silva, B. Y. K. da Silva, A. da S. N. Lopes, I. R. Guesdon, P. J. S. Maia, M. A. Abegg, G. M. Corrêa, D. F. de M. do Carmo, Chemical Composition and Biological Activities of Essential Oils from Fresh *Vismia guianensis* (Aubl.) Choisy and *Vismia cayennensis* (Jacq.) Pers. Leaves, *Research, Society and Development*, **2021**, 10, e37410817440.
- 26-A. Mermer, H. Boulebd, An eco-friendly method for the synthesis of 1,2,4-triazole-Schiff base derivatives in aqueous medium and DFT calculations, *J Mol Struct*, **2023**, 1271 doi:10.1016/j.molstruc.2022.134102.
- 27-Z. Yin, S. Li, X. Li, W. Shi, W. Liu, Z. Gao, M. Tao, C. Ma, Y. Liu, A review on the synthesis of metal oxide nanomaterials by microwave-induced solution combustion, *RSC Adv*, **2023**, 13, 3265–3277.
- 28-T. N. Moeketse, P. G. Baker, A. C. Farao, E. I. Iwuoha, Microwave-Assisted Synthesis of Schiff Base Metal–Ligand Complexes with Copper and Nickel Centres for Electrochemical In Vitro Sensing of Nitric Oxide in an Aqueous Solution, *Chemosensors*, **2022**, 10 doi:10.3390/chemosensors10050175.
- 29-P. T. Phan, J. Hong, N. Tran, T. H. Le, The Properties of Microwave-Assisted Synthesis of Metal–Organic Frameworks and Their Applications, *Nanomaterials*, **2023**, 13, 352.
- 30-A. Jain, S. De, P. Barman, Microwave-assisted synthesis and notable applications of Schiff-base and metal complexes: a comparative study, *Research on Chemical Intermediates*, **2022**, 48, 2199–2251.
- 31-N. Otani, T. Furuya, N. Katsuomi, T. Haraguchi, T. Akitsu, Synthesis of amino acid derivative Schiff base copper(II) complexes by microwave and wet mechanochemical methods, *Journal of the Indian Chemical Society*, **2021**, 98 doi:10.1016/j.jics.2021.100004.
- 32-L. Findoráková, K. Györyová, M. Melník, M. Koman, F. A. N. El-dien, K. Györyová, M. Melník, M. Koman, F. A. N. El-, Preparation, thermal decomposition, and crystal structure of Zn (II) 2-chlorobenzoate complex with nicotinamide, **2010**, 63, 3348–3355.
- 33-J. Zhang, L. Tan, W. Jiang, W. Hu, Z. Wang, N-Alkyl substituted di(perylene bisimides) as air-stable electron transport materials for solution-processible thin-film transistors with enhanced performance, *J Mater Chem C Mater*, **2013**, 1, 3200.
- 34-M. Ismael, A.-M. M. Abdel-Mawgoud, M. K. Rabia, A. Abdou, Design and synthesis of three Fe(III) mixed-ligand complexes: Exploration of their biological and phenoxazinone synthase-like activities, *Inorganica Chim Acta*, **2020**, 505, 119443.
- 35-U. Holzwarth, N. Gibson, The Scherrer equation versus the ‘ Debye – Scherrer equation ’, *Nat Nanotechnol*, **2011**, 6.
- 36-A. Abdou, Synthesis, Structural, Molecular Docking, DFT, Vibrational Spectroscopy, HOMO-LUMO, MEP Exploration, antibacterial and antifungal activity of new Fe(III), Co(II) and Ni(II) hetero-ligand complexes, *J Mol Struct*, **2022**, 1262, 132911.
- 37-A. Abdou, O. A. Omran, A. Nafady, I. S. Antipin, Structural, spectroscopic, FMOs, and non-linear optical properties exploration of three thiacai(4)arenes derivatives, *Arabian Journal of Chemistry*, **2022**, 15, 103656.
- 38-A. M. Abu-Dief, N. H. Alotaibi, E. S. Al-Farraj, H. A. Qasem, S. Alzahrani, M. K. Mahfouz, A. Abdou, Fabrication, structural elucidation, theoretical, TD-DFT, vibrational calculation and molecular docking studies of some novel adenine imine chelates for biomedical applications, *J Mol Liq*, **2022**, 365, 119961.
- 39-N. A. A. Elkanzi, A. M. Ali, M. Albqmi, A. Abdou, New Benzimidazole-Based Fe (III) and Cr (III) Complexes: Characterization, Bioactivity Screening, and Theoretical Implementations Using DFT and Molecular Docking Analysis, *Appl Organomet Chem*, **2022**, 36 doi:10.1002/aoc.6868.
- 40-A. S. El-tabl, F. A. Aly, M. M. E. Shakhofa, M. E. Adel, Synthesis, characterization, and biological activity of metal complexes of azo hydrazone ligand, *J Coord Chem*, **2010**, 63, 700–712.
- 41-C. J. Dhanaraj, J. Johnson, DNA interaction, antioxidant and in vitro cytotoxic activities of some mononuclear metal (II) complexes of a bishydrazone ligand, *Materials Science & Engineering C*, **2017**, 78, 1006–1015.
- 42-B. Singh, P. Srivastava, Studies on 2, 6-diacetylpyridine bis(2-furoylhydrazone)

- complexes of bivalent 3d-metal ions Bachcha, *Transition Metal Chemistry*, **1987**, 12, 475–477.
- 43-K. Nakamoto, Infrared and Raman Spectra of Inorganic and Coordination Compounds: Part A: Theory and Applications in Inorganic Chemistry: Sixth Edition, *Infrared and Raman Spectra of Inorganic and Coordination Compounds: Part A: Theory and Applications in Inorganic Chemistry: Sixth Edition*, **2008**, 1–419.
- 44-J. Xie, J. Qiao, L. Wang, J. Xie, Y. Qiu, An azomethine-zinc complex for organic electroluminescence : Crystal structure, thermal stability, and optoelectronic properties, *Inorganica Chim Acta*, **2005**, 358, 4451–4458.
- 45-J. Hu, J. Li, J. Qi, Y. Sun, Sensors and Actuators B: Chemical Acylhydrazone based fluorescent chemosensor for zinc in aqueous solution with high selectivity and sensitivity, *Sens Actuators B Chem*, **2015**, 208, 581–587.
- 46-K. Ouari, S. Bendia, J. Weiss, C. Bailly, Spectrochimica Acta Part A: Molecular and Biomolecular Spectroscopy Spectroscopic, crystal structural and electrochemical studies of zinc (II) -Schiff base complex obtained from 2, 3-diaminobenzene and 2-hydroxy naphthaldehyde, *Spectrochim Acta A Mol Biomol Spectrosc*, **2015**, 135, 624–631.
- 47-D. Meng, F. Liu, Y. Li, Z. Yang, G. Li, D. Guo, Synthesis, characterization and properties of salicylhydrazide-salicylacylhydrazone derivatives and their terbium complexes, *Luminescence*, **2016**, 31, 507–514.
- 48-S. Meghdadi, M. Amirnasr, Z. Azarkamanzad, K. S. JoB, F. Fadaee, A. Amiri, S. Abbasi, Benign synthesis of the unsymmetrical ligand activity, and crystal structures of Cu (II) and Zn (II) complexes, *J Coord Chem*, **2013**, 66, 4330–4343.
- 49-P. José, S. Maia, E. Medeiros, B. Maria, L. Vega, H. Nunes, Synthesis and characterization of a perylene derivative and its application as catalyst for ethanol electro-oxidation, *Chemical Papers*, **2018**, 72, 1021–1030.
- 50-E. M. Barbosa, I. S. Costa, P. H. S. de Oliveira, E. B. dos Santos, A. M. B. Silva, P. J. S. Maia, E. A. Souza, Perylene Derivative Complexes as Cocatalyst for Electrocatalytic Oxidation of Ethanol, *Revista Virtual de Química*, **2020**, 12, 1653–1661.
- 51-P. José, S. Maia, E. Medeiros, B. Maria, L. Vega, H. Nunes, Synthesis and characterization of a perylene derivative and its application as catalyst for ethanol electro-oxidation, *Chemical Papers*, **2018**, 72, 1021–1030.
- 52-P. José, S. Maia, J. Ferreira, C. Flávio, A. De Freitas, Photophysical properties of a perylene derivative for use as a catalyst in ethanol electrooxidation, *Research on Chemical Intermediates*, **2019**, 45, 5451–5472.
- 53-S. P. Mohammed, B. Namsheer, Dr. J. Harindran, B. Thomas, M. K. Sebastian, Evaluation of Analgesic And Anti Oxidant Activities of Schiff Bases, *European Journal of Pharmaceutical and Medicinal Research*, **2016**, 3, 418–424.
- 54-M. Hanif, M. Hassan, M. Rafiq, Q. Abbas, A. Ishaq, S. Shahzadi, S. Seo, M. Saleem, Microwave-Assisted Synthesis, In Vivo Anti-Inflammatory And In Vitro Antioxidant Activities, And Molecular Docking Study Of New Substituted Schiff Base Derivatives, *Pharm Chem J*, **2018**, 52, 424–437.
- 55-S. P. Mohammed, B. Namsheer, Dr. J. Harindran, B. Thomas, M. K. Sebastian, Evaluation Of Analgesic And Anti Oxidant Activities Of Schiff Bases, *European Journal of Pharmaceutical and Medicinal Research*, **2016**, 3, 418–424.
- 56-R. S. Shivhare, D. K. Mahapatra, R. R. Nair, S. N. Deshmukh, Schiff's base derivatives of murrayanine demonstrated enhanced antioxidant activity than its parent moiety, *Indian Journal of Pharmaceutical Education and Research*, **2016**, 50, 598–604.
- 57-V. Gorantla, R. Gundla, S. S. Jadav, S. R. Anugu, J. Chimakurthy, S. K. Nidasanametla, R. Korupolu, Molecular hybrid design, synthesis and biological evaluation of N-phenyl sulfonamide linked N-acyl hydrazone derivatives functioning as COX-2 inhibitors: New anti-inflammatory, antioxidant and anti-bacterial agents, *New Journal of Chemistry*, **2017**, 41, 13516–13532.
- 58-M. de Freitas Silva, E. T. Lima, L. Pruccoli, N. G. Castro, M. J. R. Guimarães, F. M. R. da Silva, N. F. Nadur, L. L. de Azevedo, A. E. Kümmerle, I. A. Guedes, L. E. Dardenne, V. S. Gontijo, A. Tarozzi, C. Viegas, Design, synthesis and biological evaluation of novel triazole N-acylhydrazone hybrids for Alzheimer's disease, *Molecules*, **2020**, 25 doi:10.3390/molecules25143165.
- 59-C. G. L. Nongpiur, L. Dkhar, D. K. Tripathi, K. M. Poluri, W. Kaminsky, M. R. Kollipara, Half-sandwich platinum group metal complexes containing coumarin-N-acylhydrazone hybrid ligands: Synthesis and biological evaluation studies, *Inorganica Chim Acta*, **2021**, 525 doi:10.1016/j.ica.2021.120459.
- 60-C. G. L. Nongpiur, D. F. Diengdoh, N. Nagar, K. M. Poluri, P. M. Gannon, W. Kaminsky, M. R. Kollipara, Mono and dinuclear ruthenium, rhodium and iridium metal complexes containing N-acylhydrazone moiety: Synthesis and in vitro biological studies, *Polyhedron*, **2022**, 221 doi:10.1016/j.poly.2022.115855.
- 61-N. Belkheiri, B. Bouguerne, F. Bedos-Belval, H. Duran, C. Bernis, R. Salvayre, A. Nègre-Salvayre, M. Baltas, Synthesis and antioxidant activity evaluation of a syringic hydrazones family, *Eur J Med Chem*, **2010**, 45, 3019–3026.